COMMUNICATIONS CHEMISTRY

ARTICLE

https://doi.org/10.1038/s42004-020-00396-9 OPEN

Hydrogen release from a single water molecule on V_n^+ $(3 \leq n \leq 30)$

Hanyu Zhang [1,4], Haiming Wu[1,4], Yuhan Jia[1,2], Baoqi Yin[1,2], Lijun Geng[1], Zhixun Luo [1,2✉] & Klavs Hansen [3]

Water and its interactions with metals are closely bound up with human life, and the reactivity of metal clusters with water is of fundamental importance for the understanding of hydrogen generation. Here a prominent hydrogen evolution reaction (HER) of single water molecule on vanadium clusters V_n^+ $(3 \leq n \leq 30)$ is observed in the reaction of cationic vanadium clusters with water at room temperature. The combined experimental and theoretical studies reveal that the wagging vibrations of a V-OH group give rise to readily formed V-O-V intermediate states on V_n^+ $(n \geq 3)$ clusters and allow the terminal hydrogen to interact with an adsorbed hydrogen atom, enabling hydrogen release. The presence of three metal atoms reduces the energy barrier of the rate-determining step, giving rise to an effective production of hydrogen from single water molecules. This mechanism differs from dissociative chemisorption of multiple water molecules on aluminium cluster anions, which usually proceeds by dissociative chemisorption of at least two water molecules at multiple surface sites followed by a recombination of the adsorbed hydrogen atoms.

[1] Beijing National Laboratory of Molecular sciences (BNLMS), State Key Laboratory for Structural Chemistry of Unstable and Stable Species, Institute of Chemistry, Chinese Academy of Sciences, Beijing 100190, P.R. China. [2] University of Chinese Academy of Sciences, Beijing 100049, P.R. China. [3] Joint Centre for Quantum Studies and Department of Physics, School of Science, Tianjin University, Tianjin, P.R. China. [4] These authors contributed equally: Hanyu Zhang, Haiming Wu. ✉email: zxluo@iccas.ac.cn

Generating hydrogen from water is one of the attractive research fields motivated by the quest for sources of clean energy in modern society[1,2]. Numerous strategies have been developed for hydrogen production including electrolysis[3–5], artificial photosynthesis[6], use of photocatalysts[7,8], and thermal decomposition of water[9]. In the ongoing efforts devoted to exploring effective catalysts and cluster supports for water splitting[10–13], aluminium alloy powders with unique nanoscale galvanic microstructure have been shown to produce hydrogen gas upon contact with water[14]. Also, hydrogen elimination from Al-based hydrates, e.g., $[Al, 20H_2O]^+$, were proposed in previous studies[15–17], where the proton transfer in the water cluster network enables a migrated proton to recombine with a hydridic H at the Al^{III} cation, and a joint experimental and theoretical study illustrated the potential application of pure aluminium cluster anions for effective production of H_2 from water[18]. In these experiments, active sites on the surface of the aluminium clusters, typically Al_{16}^-, Al_{17}^-, and Al_{18}^-, produced hydrogen from contact with water at room temperature. These reactions are initiated by dissociative chemisorption of a few water molecules at different surface sites, and continues by the Tafel reaction mechanism of recombination of adsorbed hydrogen atoms (i.e., $H_{ad} + H_{ad} \rightarrow H_2$)[19,20]. In a further development, the complementary-active-sites (CAS) mechanism[18] has been established to rationalize the size-selective reactivity of Al clusters with polar molecules beyond water[21–26] and have demonstrated the existence of competition of water versus alcohols in reactions with Al clusters[27], have illustrated how partial atomic charges and bonding orbitals[28] and the doping of heteroatoms affects such HER processes[29–33], and have demonstrated the Eley–Rideal and Langmuir–Hinshelwood mechanisms in the presence of two OH-group molecules[34].

Such advances have stimulated further studies of cluster reactivity of transition metal clusters in view of their *d*-electron activity. As an important family of functional materials, transition metal oxides show high propensity for a variety of catalytic reactions, including oxygen evolution reactions. Also, the interactions of light transition metal cations with compounds containing prototypical bonds (e.g., N–H, O–H) have attracted a great deal of attention over the past years[35–39]. For example, a study of the hydrated vanadium cations has shown that absorption of ambient blackbody radiation enables O-atom transfer from H_2O to metal, followed by hydrogen evolution[40–42]. Also, vanadium ions in their ^3F and other higher lying states were found to react with water[40,43], however, for the ground-state cation (V^+, ^5D) which is ~1.08 eV lower in energy[44,45], the H_2 release suffers from a large energy barrier due to the absence of active sites. As the binding energies of $V_n^+H_2O$ ($n = 2$–13) are much smaller than that of V^+H_2O[46], this opens the possibility that similar mechanisms can be present for clusters, which is what motivated the present studies of the HER efficiency on V_n^+ clusters.

For the experiments reported here, we have prepared mass-resolved cationic vanadium clusters (V_n^+) and have observed their reactions with water vapour in a compact flow tube reactor. The composition of the reaction products were measured with a homemade reflection time-of-flight mass spectrum (Re-TOFMS)[47]. Three series of reaction products, V_nO^+, $V_nO_2^+$ and $V_nO_3^+$, were identified, corresponding to successive reactions of V_n^+ with H_2O molecules. Both the monomer and dimer, $V_{1,2}^+$, are found to be inert towards water; in contrast, the clusters $V_{n\geq3}^+$ (especially V_5^+ and V_9^+) readily react and result in dehydrogenation products, specifically by the reaction $V_{3\leq n\leq30}^+ + H_2O \rightarrow V_nO^+ + H_2$. Supported by density functional theory (DFT) calculations, we have interpreted the origin of this strongly size-dependent reactivity with its onset at $n = 3$. Analyses of the detailed energetics and reaction dynamics suggest that a three-atom synergistic effect and the presence of wagging vibrations of hydroxyl groups that facilitate the reactions of the formed V–O–V intermediate states and that allow the terminal hydrogen to interact with adsorbed hydrogen atom thus enabling facile hydrogen release (i.e., $H_{ad} + H_{hydroxyl} \rightarrow H_2$). Notably, this mechanism works without having to transfer two hydrogen atoms onto the metal surfaces, similar to an electrochemical Heyrovsky reaction (i.e., $H^+(\text{or } H_2O) + H_{ad} + e^- \rightarrow H_2(\text{or } H_2 + OH^-)$)[20,27,48]. Such three-atom enhanced reactivity was also used to describe the Pt_3 cluster catalysis in N–H dissociation[49].

Results

Mass spectrometric analysis. Figure 1a presents a typical mass spectrum of the as-prepared cationic vanadium clusters V_n^+ ($n = 1$–30) generated in a customized laser evaporation (LaVa) source with He as the buffer gas (1 MPa). To such spectra, different amounts of heavy-oxygen water ($H_2{}^{18}O$) were introduced as the reactant. The water vapour (~2% $H_2{}^{18}O$ in He) was introduced into the (downstream) flow-tube reactor by a pulse valve along with helium carrier gas (0.1 MPa). The reaction products with the thermalized V_n^+ clusters are shown in Fig. 1b–d. Firstly, the products $V_nH_2{}^{18}O^+$, $V_n{}^{18}O^+$, and $V_n{}^{18}O_2^+$ suggest that the adsorption of water and the release of hydrogen occur on the vanadium clusters sequentially. Secondly, we observe that in parallel with an increasing concentration of $H_2{}^{18}O$, pure metal clusters are consumed and at the same time, the adsorption and dehydrogenation products emerge gradually. It is clear from this trend that V_n^+ clusters readily react with water to form vanadium oxides via an adsorption–dissociation process followed by H_2 release. Thirdly, the spectra can be divided into three regions according to the nature of the products as follows: (i) no reaction product of V_1^+ and V_2^+ was observed under the conditions of our experiment; (ii) vanadium oxides of V_{3-10}^+ are easily formed with a small number of adsorption products observed; (iii) for $V_{n\geq10}^+$, the $V_nH_2{}^{18}O^+$ series dominates the reaction products. We describe these three distinct regions to the size dependence of the reactivity of V_n^+ clusters with water. (For comparison experiments of the deuterium water and He collision see Supplementary Figs. 3 and 4.)

The inset graph in Fig. 1 gives a close-up view of V_n^+ ($n =$ 3–16) reacting with a relatively large amount of $H_2{}^{18}O$ in which it can be clearly seen that V_n^+ clusters react with H_2O to form $V_nH_2O^+$, V_nO^+, $V_nOH_2O^+$, $V_nO_2^+$ and $V_nO_3^+$. Among these five types of products, V_nO^+ and $V_nO_2^+$ shows the highest and second-highest mass abundances, respectively, indicating that H_2 release dominates the reaction pathways of $V_{n\geq3}^+$ with water. In comparison, the relatively lower mass intensities of $V_nOH_2O^+$ presumably correspond to the intermediates of a successive reaction of V_nO^+ with a second H_2O molecule that ultimately may lead to the removal of the second H_2. The observation of $V_nO_3^+$ shows the ability of V_n^+ to produce three H_2 molecules by consuming three H_2O molecules. There are no higher order oxides observed with our experimental condition. The observed reactions can be summarized as

$$V_n^+ + H_2O \rightarrow V_nH_2O^+, \quad (1)$$

$$V_n^+ + H_2O \rightarrow V_nO^+ + H_2, \quad (2)$$

$$V_n^+ + 2H_2O \rightarrow V_nOH_2O^+ + H_2, \quad (3)$$

$$V_n^+ + 2H_2O \rightarrow V_nO_2^+ + 2H_2, \quad (4)$$

$$V_n^+ + 3H_2O \rightarrow V_nO_3^+ + 3H_2. \quad (5)$$

Considering the above five reaction channels together and noting that the water concentration exceeds the cluster concentration in the beam, the observed reaction of

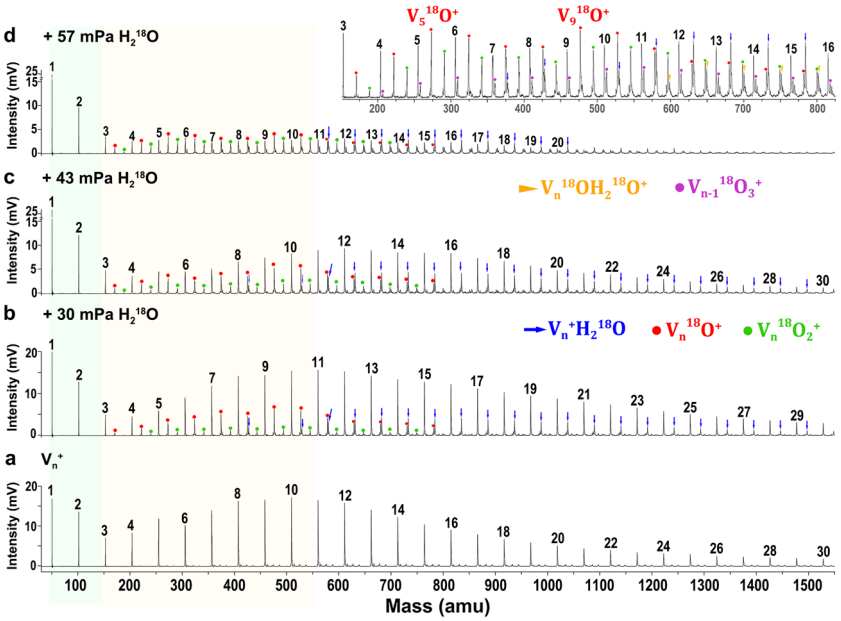

Fig. 1 Mass spectrometry observation. Mass spectra of **a** cationic vanadium clusters and **b**–**d** V_n^+ ($n = 1$–30) reacting with different amounts of $H_2{}^{18}O$. The partial pressures of $H_2{}^{18}O$ vapour are ~30, ~43, and ~57 mPa, respectively, corresponding to an average number of collisions at 4.4, 6.4, and $8.3 \times 10^3\ s^{-1}$. Insets gives a close-up view of **d**. The pure vanadium clusters are labelled by numbers, vanadium monohydrates are labelled by blue arrows, vanadium monoxides are labelled by red circles, vanadium dioxides are labelled by green circles, vanadium trioxides are labelled by purple circles, and hydrated vanadium monoxides are labelled by yellow triangles.

"$V_n^+ + m(H_2O) \rightarrow V_nO_x(H_2O)_{m-x}^+ + xH_2 (m \geq 1)$" is tentatively described as a pseudo-first-order reaction concerning the depletion of the bare metal clusters. No claim is made about the order of the subsequent reactions. The pseudo-first-order rate constants (k_1) for this reaction can be estimated by the following Eq. (6):

$$\ln\frac{I_n}{I_s} = -k_1\frac{P_e\Delta t}{k_B T} = \ln\frac{I(V_n^+)}{I(V_n^+ + V_nO^+ + V_nH_2O^+ + V_nOH_2O^+ + V_nO_2^+ + V_nO_3^+)}, \quad (6)$$

$$k_1^{rel}(n) = k_1(V_n^+)/k_1(V_{14}^+) \quad (7)$$

in which the variable I_n stands for the integrated intensity of the parent peaks at a certain gas pressure, and I_s refers to the sum of integrated peaks intensities of both the reactants and products. The chemical symbols on the right-hand side represent the measured mass spectrometric intensities. The constants P_e, k_B, and T refer to the pressure of the reactant, Boltzmann's constant, and the reaction temperature (298 K). Δt is the effective residence time in the reactor (~60 μs). The relative values of the rate constants $k_1^{rel}(n)$ defined by Eqs. (6) and (7) are plotted in Fig. 2 (for more details see Supplementary Figs. 1 and 2 and Supplementary Table 1). As is seen, except for V_1^+ and V_2^+ that have a reaction rate close to zero based on the mass spectrometry observation in this study, the k_1^{rel} values of the V_n^+ ($3 \leq n \leq 20$) illustrate size-dependent reaction rates with local smaller values at $n = 3$, 6 and 16. Further, considering the hydrogen evolution channels (Eqs. (2)–(5)) together, also plotted (red) in Fig. 2 is the relative mass abundances of a sum of the HER products (and also seen directly from the mass abundances in Fig. 1), the water dehydrogenation channel has a local maximum for V_5^+ and V_9^+.

Structure identification and energetics analysis. In order to elucidate the origin of the pattern of relative stability, reactivity and the H_2 release mechanism, ground state structures of V_n^+, V_nO^+, and $V_nH_2O^+$ ($n = 1$–13) have been optimized and calculated quantum chemically at the BP86-D3/def2-TZVP level of theory via Gaussian 09 suite of programmes (more results are given in Supplementary Tables 2–6 and Supplementary Figs. 5–7). The lowest energy structures determined for $V_nH_2O^+$ have the following features: (i) water adsorption on V_n^+ proceeds through vertex V−O coordination modes (Fig. 3a); (ii) the electronic and geometric structures of the V_n^+ clusters are preserved to a large extent when forming $V_nH_2O^+$. In addition, the adsorption energies of H_2O onto V_n^+ ($E_{ad} = E(V_nH_2O^+) - E(V_n^+) - E(H_2O^+)$) display a dramatic size dependence. The E_{ad} of V_1^+ is substantially higher than the values for the V_n^+ clusters, indicating the relative stability of $V_1H_2O^+$ and hence explains the suppression of H_2 release from the complex. This $V_nH_2O^+$ binding energetics is in concordance with a previous study[46], the water-binding energies decrease from $n = 1$ to 4 and show an odd–even oscillation for $n = 3$–13. Considering that the positions of the water molecules are quite external from the clusters, without any significant rearrangement of the cluster geometry, the odd–even effect in the binding energy of the water molecule to the V_n^+ cluster reflects a similar effect in the bare cluster dissociation energy, albeit with a factor-of-ten smaller amplitude. Similar odd–even effects have been seen in clusters of alkali and coinage metals[50–52], where the prevailing interpretation is that it arises as a consequence of Jahn–Teller distortion combined with oscillating spin degeneracy.

It is noteworthy that the most exothermic reaction appears at the size ($n = 5$) where also 3D structures appear as the energy minima found in this study. The close relation between geometry and reactivity surmised is corroborated by Fig. 3b which summarizes the bond angle of O–V–V and the dihedral angle

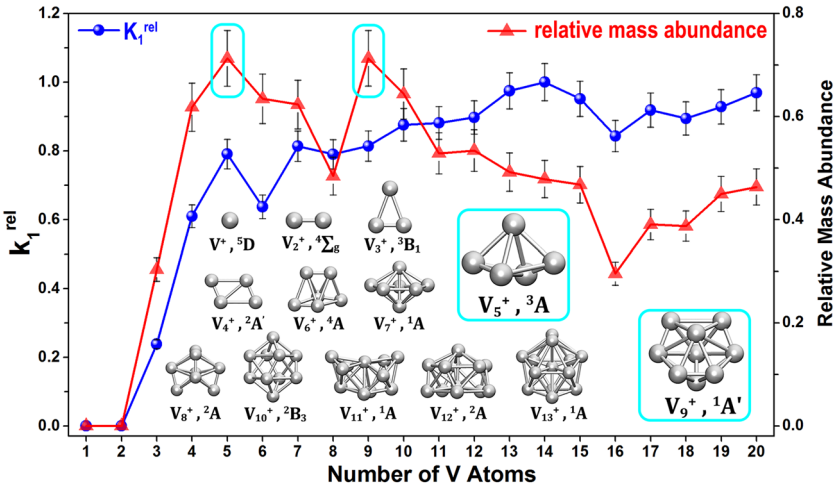

Fig. 2 Experimental analysis. (Blue circles) The normalized rate constants relative to the maximum value for the reactions of V_n^+ ($n = 1$–20) with $H_2{}^{18}O$ which are defined as $k_1^{rel} = k_1(V_n^+)/k_1(V_{14}^+)$. (Red triangles) The relative mass abundances which are defined as $I(V_nO^+ + V_nOH_2O^+ + V_nO_2^+ + V_nO_3^+)/I(V_n^+ + V_nO^+ + V_nH_2O^+ + V_nOH_2O^+ + V_nO_2^+ + V_nO_3^+)$. The insets show the structures and electronic states of ground state V_n^+ clusters. The uncertainties of rate constant estimation and relative intensities are given by the uncertainties in the integration of the mass peaks.

of O–VV–V in the $V_nH_2O^+$ series. Generally speaking, the smaller the ∠O–V–V and φ O–VV–V values are, the more easily the H_2O molecule will bend over a triangular face of V_n^+ and hence promote HER processes. Conversely, the linear shape of $V_1H_2O^+$ and $V_2H_2O^+$ and the strong interaction between metal and water impede the bending of the V–O bond. In comparison, the dihedral angle φ O–VV–V in $V_5H_2O^+$ is the smallest among the $V_nH_2O^+$ series, indicating an efficient HER process leading to the formation of V_5O^+. Also, $V_9H_2O^+$ has the smallest bond angle ∠O–V–V in the series, as well as a relatively small dihedral angle φ O–VV–V, which facilitates wagging vibrations of the V–OH_2 (Supplementary Fig. 8) and thus benefits the formation of V–O–V intermediate states according to this scheme. This provides a reasonable explanation for the preponderance of V_9O^+ products in the mass spectra.

Figure 3c presents the lowest energy structures of the V_nO^+ clusters after the hydrogen release, as well as the O-binding energies ($E_{O-binding} = E(V_nO^+) - E(V_n^+) - E(O)$) and thermodynamic energy changes for the hydrogen evolution reaction (Δ_rH_0) defined by $\Delta_rH_0 = [E(V_nO^+) + E(H_2)] - [E(V_n^+) + E(H_2O)]$, where the E all correspond to the zero-point-vibration corrected total energies in their ground states. This figure therefore shows the thermodynamics tendency of the H_2 evolution with size. It is seen that V–O shows a bonding energy at about 6.76 eV, which is consistent with the previously published studies of dissociation energy of V–O bond at ~6.48 ± 0.09 eV[53,54], although the value deduced from threshold analysis of dissociation reaction at 5.99 eV[54], due to likely systematic error on nonthermalized state. V_2O^+ and V_3O^+ take on a planar V–O–V structure with C_{2v} symmetry, which can be constructed by capping an oxygen atom on the V–V edge. In contrast, for all the other V_nO^+ ($n = 4$–13) clusters, the O atom is attached to one of the triangular faces of V_n^+. Furthermore, the energy release for reaction with V_1^+ and V_2^+ is much less than that of V_3^+ to V_{13}^+, which supports the absence of VO^+ and V_2O^+ in the mass spectra. DFT-calculated energetics including V-atom dissociation energies, H_2O-binding energy and O-binding energies etc., along with a comparison to those in literatures, are provided in Supplementary Tables 7–10 and Supplementary Figs. 9–12. Besides, a reasonable HER of water on metals is associated with the ability to donate (or accept) electrons to (or from) the molecules, including initial steps of the "$V_n^+ + H_2O$", the activation and rupture of the O–H bond. From the natural population analysis (NPA) of charges on H_2O in $V_nH_2O^+$ clusters (Supplementary Fig. 13), it is seen that V_9^+ has the highest amount of electron transfer, consistent with its outstanding reactivity. More details showing the energy decomposition analysis is provided in Supplementary Table 12 and Supplementary Fig. 16.

HER mechanism. Having determined the thermodynamics of HER of these V_n^+ clusters, Fig. 4 presents a comparison of the energetics of the reaction coordinates for "$V_{1-3}^+ + H_2O \rightarrow V_nO^+ + H_2$". For V^+ (Fig. 4a), the ground electronic state is $V^+(^5D)$ which displays a M^+–OH_2 bond energy of 1.86 eV, which is consistent with the previous studies by Armentrout and colleagues[55]. The adsorption products (I_1) comply with the spin conservation for triplet and quintet potential energy surfaces (PESs), while the TS_1 of spin-triplet state lies below the energy of the spin-quintet state by 0.19 eV, likely leading to a spin crossing before the subsequent reaction steps. However, there remains the large energy barrier of 1.76 eV for the hydrogen atom transfer to V^+ required for the production of the HV^+OH intermediate (I_2). The second hydrogen transfer from oxygen to the metal takes place through TS_2. This transition structure leads to another intermediate found on the reaction path, the H_2VO^+ complex (I_3). From this intermediate, the loss of H_2 proceeds without a transition structure to the observed major products, VO^+ and H_2[40]. It should be noted that there is a $V^+(^3F)$ state which is 1.08 eV higher in energy than $V^+(^5D)$, consistent with previously reported results[44,45]. Nevertheless, an initial spin excitation of $V^+(^5D)$ to $V^+(^3F)$ could promote the HER processes, as was observed in the previous study involving black body radiation[41]; otherwise, the thermalized downstream reaction of ground-state $V^+(^5D)$ with water could not be enabled even though this reaction is exothermic. Considering that the clusters in this study are close to thermal equilibrium, and that under the ambient conditions, the 1.76 eV energy barrier is unsurmountable for thermalized V^+ ions due to the good equilibration with the helium buffer gas, a total reaction exothermicity notwithstanding. The large energy barrier of the transition structure for the first-step hydrogen transfer was also identified by previous studies,

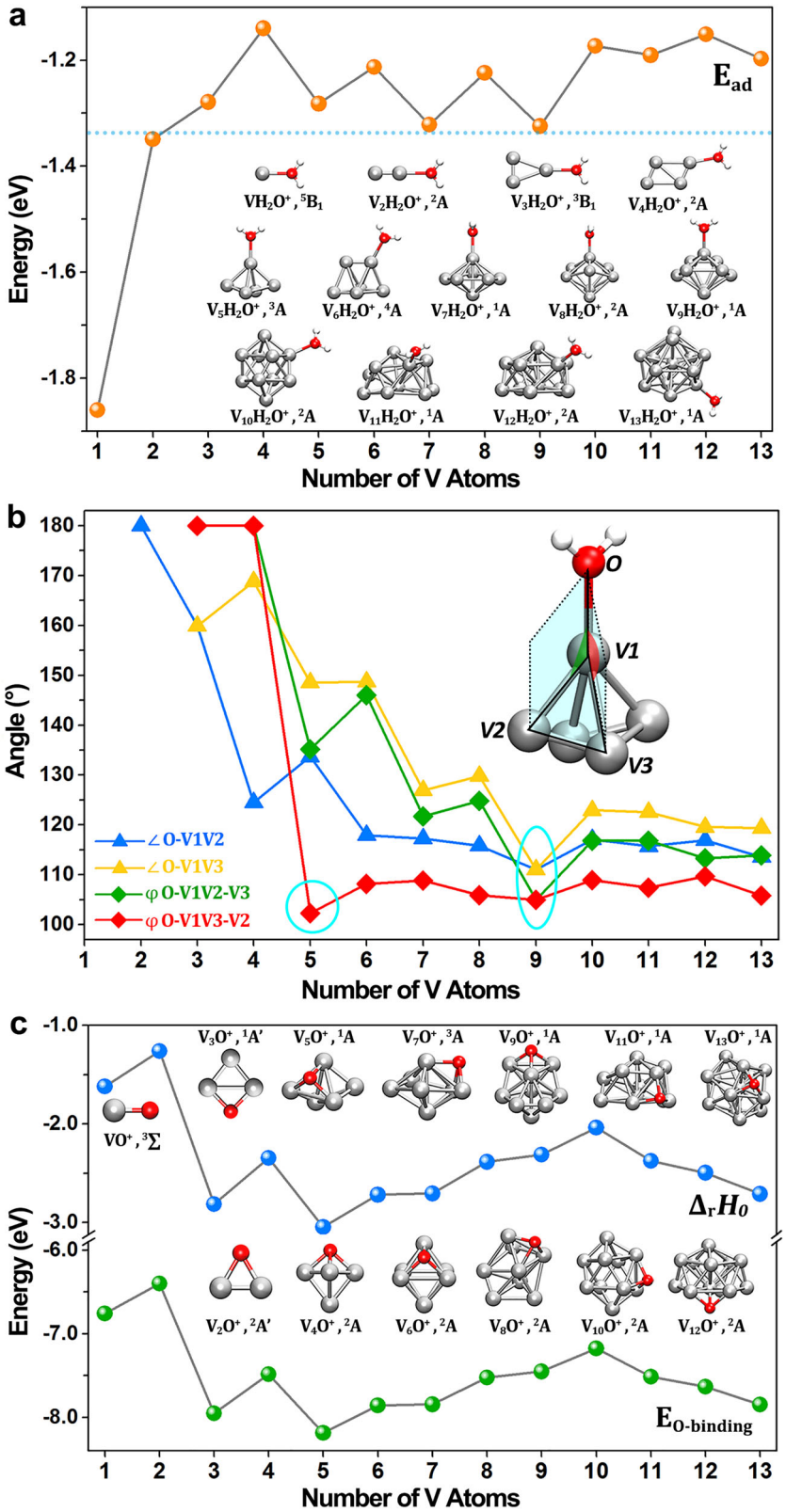

Fig. 3 Structures and energetics. a Adsorption energy of V_n^+ and H_2O ($E_{ad} = E(V_nH_2O^+) - E(V_n^+) - E(H_2O^+)$). **b** Bond angles on the lowest energy structures of $V_nH_2O^+$ clusters. The inset gives the definition of bond angle (∠O-V-V, blue and orange dots) and dihedral angle (φ O-VV-V, green and red dots). The V atom adsorbing the water molecule is defined as V-1, the V-2 corresponds to the one with the largest positive partial charge, while V-3 is at the minima. **c** The O-binding energies ($E_{O\text{-binding}}$, green dots) of O to V_n^+, and the zero-point-vibration corrected total energies of the hydrogen evolution reaction (Δ_rH_0, blue dots) of V_n^+ ($n = 1$–13) with H_2O, where the values are just shifted with the same energy determined by the H_2O reactant and H_2 product. The insets show the lowest energy structures of $V_nH_2O^+$ and V_nO^+.

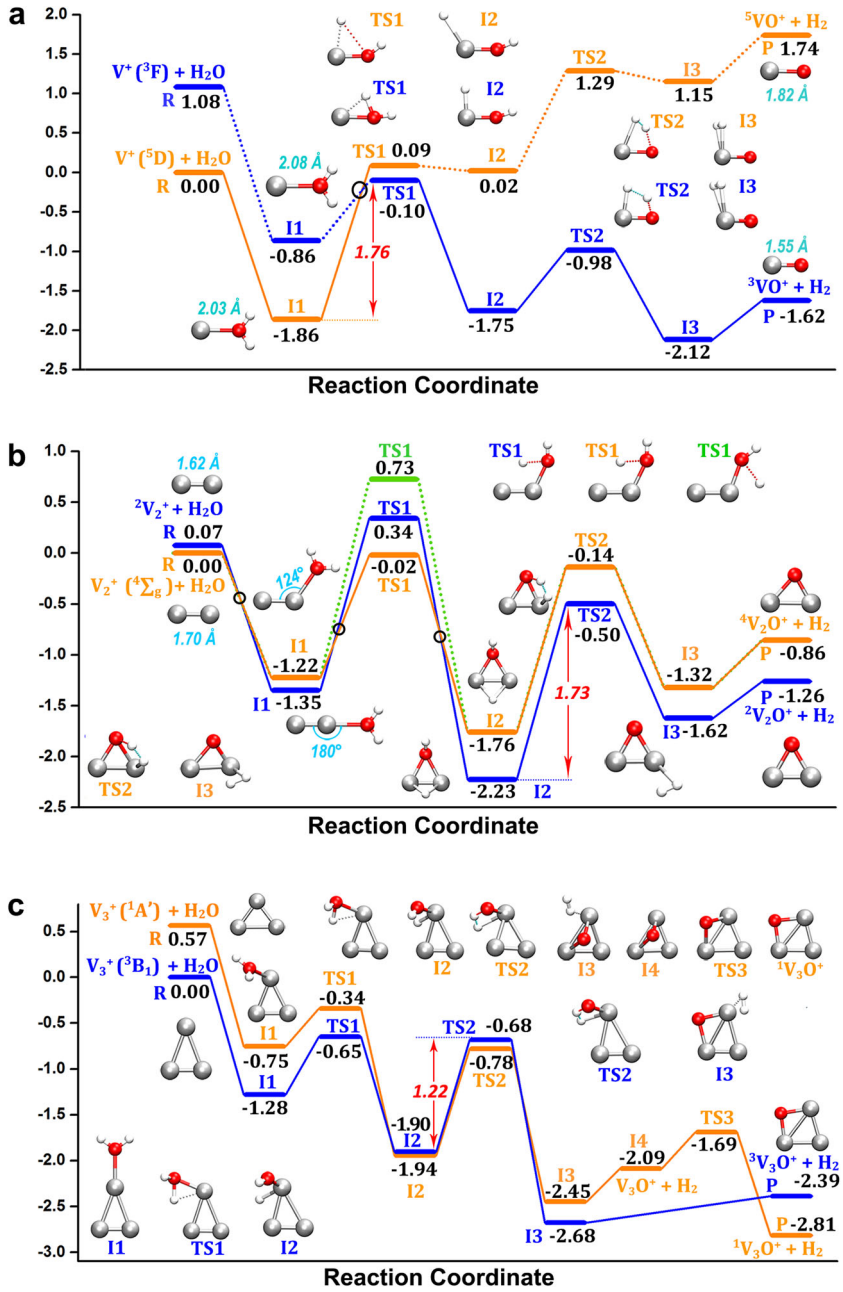

Fig. 4 Reaction coordinates of HER on V_{1-3}^+. Reaction coordinates of **a** "$V_1^+ + H_2O \rightarrow V_1O^+ + H_2$", **b** "$V_2^+ + H_2O \rightarrow V_2O^+ + H_2$" and **c** "$V_3^+ + H_2O \rightarrow V_3O^+ + H_2$". The bond lengths and bond angles are labelled in cyan. The energy values are relative to the entrance channel, corrected with zero-point vibration energies, and given in eV. Spin multiplicity is marked as pre-superscript. The black circles stand for spin inversion.

e.g., with a value of 2.23 eV in the work of A. Irigoras et al. [40]. Therefore, the large energy barrier in the first-step hydrogen transfer impedes the production of triplet VO^+, in good agreement with our mass spectrometry observations.

For V_2^+, we investigated two reaction pathways, considering the spin multicity of V_2^+, as shown in Fig. 4b where a blue line indicates the path of doublet V_2^+ and an orange the quartet V_2^+ path. Between I_1 and TS_1, the two spin states change energy-ordering resulting in spin crossing for the blue and orange paths. Considering that the energies of quartet and doublet V_2^+ are close (0.07 eV), the first hydrogen transfer is a two-state step[56] with spin inversion occurring twice. In addition, another possible path is offered by transferring the first H atom to the V atom ($^4V_2^+$, green line). The rate-determine step in the reaction of "$V_2^+ + H_2O$" is the second hydrogen transfer with a barrier of 1.73 eV which is difficult to cross, mainly due to the stability of I_2 intermediate state. Thus, we ascribe the absence of V_2O^+ in the mass spectra to the large energy barriers of transition structures although overall this reaction itself is thermodynamically favourable. We reiterate the observation that the presence of the helium gas plays an essential role for this conclusion. In the absence of a thermalizing agent, the determining parameter would be the overall exothermicity of the reaction.

The case of V_3^+ (Fig. 4c) represents a very different situation from that of $V_{1,2}^+$. The spin multiplicity for the lowest energy structures of $^1V_3O^+$, also differs from that of the bare cluster, $^3V_3^+$, and two reaction pathways are considered. A difference to $V_{1,2}^+$ is that the first hydrogen barrier is much lower for V_3^+

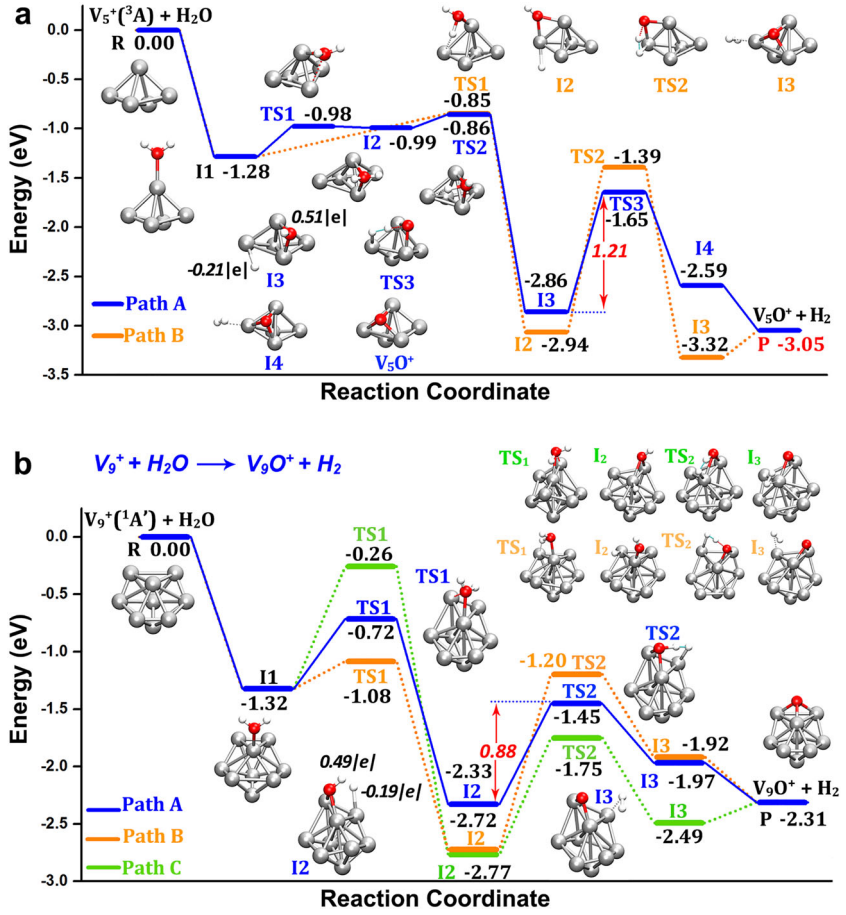

Fig. 5 Reaction coordinates of HER on V_5^+ and V_9^+. a The reactions of "$V_5^+ + H_2O \rightarrow V_5O^+ + H_2$", and **b** "$V_9^+ + H_2O \rightarrow V_9O^+ + H_2$". The energy values are relative to the entrance channel and are given in eV. The marked partial charges on hydrogen atoms of the intermediates (HV_5OH^+ and HV_9OH^+) are calculated at BP86-D3/def2-TZVP level of theory using NBO 6.0 method[73].

than that of $V_{1,2}^+$ due to a significantly decreased bond angle ∠O–V–V in $V_3H_2O^+$, as discussed above. This allows wagging vibrations of the hydroxyl group and thus the formation of V–O–V intermediates. The second hydrogen transfer is the rate-determine step with a barrier of 1.22 eV. Also, this value is smaller than the rate-determine step in $V_{1,2}^+$, indicating a feasible HER for V_3^+ clusters. For reaction coordinate of "$V_3^+ + 2H_2O \rightarrow V_3O_2H_2^+ + H_2$" see Supplementary Fig. 17.

The reaction of V_5^+ shows a similar behaviour. Figure 5a displays the reaction coordinates for the reaction $V_5^+ + H_2O \rightarrow V_5O^+ + H_2$, where the small dihedral angle of O–VV–V in the ground state structure of $V_5H_2O^+$ benefits the first hydrogen transfer to produce the HV_5OH^+ intermediate (I_3, blue line). In this intermediate state, the O atom bridges two V atoms and the H atom is connected with the third V atom in the V–V–V plane. Subsequently H_2 releases from the third V atom via TS_3 with an energy barrier of 1.21 eV. The relatively low transition structure energy and the largely exothermic final product V_5O^+ accounts for its reasonable mass abundance in the experimental observation. It is important to notice that the reaction pathway without the participation of the third V atom in the triangle (orange line) has a larger barrier in the rate-determining step, which once more illustrates the importance of cooperation of the third vanadium atom in the V_n^+ cluster reactions with water. Note that the LUMO energy level of V_5^+ is close to HOMO level of H_2O, which could benefit the V_5^+–H_2O orbital interactions (Supplementary Figs. 14 and 15).

To investigate the generality of this principle, we have also calculated the reaction coordinates for "$V_9^+ + H_2O \rightarrow V_9O^+ + H_2$", which is shown in Fig. 5b. Among the three possible pathways, the one marked with blue line exhibits a fairly low barrier (0.88 eV) from HV_9OH^+ (I_2) to $H_2V_9O^+$ (I_3). Again, the pathway of V_9^+ HER demonstrates the importance of the presence of three V atoms, two of which form a V–O–V bridge in the $H_2V_nO^+$ intermediate and the third provides the hydrogen receptor and the H_2 removal site. Similar to the reaction paths of "$V_5^+ + H_2O$", the O-atom capping on the V–V–V triangle plane is formed in $H_2V_9O^+$ after a two-step hydrogen transfer with the second step the rate-determining one. The mass spectrometry observation (Fig. 1) reveals that V_9O^+ dominates the reaction products, with rare $V_9(H_2O)^+$ product being observed, which coincides with the fairly low barrier and also large NPA charge transfer in $V_9(H_2O)^+$ (Supplementary Fig. 13 and Supplementary Table 11), indicating high HER activity of V_9^+. In comparison, there is relatively lower HER activity for V_n^+ with $n > 10$, although they do react and form water-addition products. This could be associated with the higher density of vibrational states, providing a more efficient dissipation of the association energy, in combination with a longer time for H atoms to reach the proper site to complete H–H recombination.

Discussion

The gas-phase reactivity of cationic vanadium clusters V_n^+ towards water has been studied experimentally and theoretically. A significant H_2 release is observed for $n \geq 3$, deduced from reaction products observed in the mass spectra. Analyses of the mass abundances, energetics and reaction dynamics indicate the inertness of $V_{1,2}^+$ towards water at room temperature. In contrast, the HER is significant for V_3^+, V_5^+ and V_9^+, processes that point to the H_2 release mechanism from such transition metal cluster cations. The first step in the HER is the formation of the $V_nH_2O^+$ complex, followed by the displacement of one hydrogen atom from oxygen to the metal cluster, reaching the HV_n^+OH molecule through a transition structure TS_1. This dissociative chemisorption step has similarities to the reaction of main group metal clusters with alcohols, but still differs as the transition metal clusters arrange with a V–O–V bridge for the I_2 intermediate state. At the second transition structure, the remaining hydrogen atom can either transfer from oxygen to the metal through a second transition structure TS_2 or interact directly with the adsorbed H atom. Both cases lead to a facile HER process "$H_{ad} + H_{hydroxyl} \rightarrow H_2$". Furthermore, the final intermediates of $H_2V_nO^+$ complexes allow the oxygen to bond with three vanadium atoms, which is associated with a highly exothermic product. In this mechanism, the bond angle of O–V–V and dihedral angle of O–VV–V in $V_nH_2O^+$ complex plays a pivotal role for the HER reaction process. The formation of a V–O–V bridge and the participation of the third V atom for H attachment in HV_n^+OH molecule are the determinants of the energy barriers. The distinct difference from the reactions of aluminium-based clusters is that a V_n^+ cluster only needs one water molecule to generate a hydrogen molecule. Thus, this study not only updates the HER mechanism on metals, but also hints at a strategy to design materials that could supply portable fuel cells of hydrogen.

Methods

Experimental methods. The home-made reflection time-of-flight mass spectrometer (Re-TOFMS)[47] equipped with a fast-flow reaction tube was utilized to conduct the gas-phase experiments of the cationic vanadium clusters V_n^+ reacting with heavy-oxygen water (2% $H_2{}^{18}O$/He). The heavy oxygen isotope (oxygen-18) was used to clear the mass spectroscopic identification of water reaction products without interference of trace oxygen contamination (oxygen-16) in the vacuum chamber. A brief description of the apparatus is given here while detailed information can be found in our previously published studies[44,57]. The vanadium clusters (V_n^+) were generated in the cluster formation channel after laser ablation of a vanadium disk (99.9% purity), with He (99.999%, 1.0 MPa backing pressure) as the buffer gas. After ablation and cluster generation, the molecular beam flowed through a nozzle to the reaction tube where 2% $H_2{}^{18}O$/He was injected by a pulsed general valve (Parker, Serial 9). The amount of $H_2{}^{18}O$ was controlled by varying the on-time pulse width of the reaction gas injection. At the end of the reaction chamber, the molecular beam was skimmed, differentially pumped and entered the TOF chamber for mass spectrometry analysis. The molecular density of the reactant gas (ρ, molecule m^{-3}) was experimentally controlled and determined by $\rho = N/(t \cdot \upsilon \cdot S)$, in which N is the number of reaction gas molecule per pulse, t is the pulse duration, S and υ are the cross-sectional areas defined by the inner diameters of the reaction-tube and the flowing velocity of cluster beam in the reactor. From these numbers, the value of ρ in this study were calculated to be $0.7 \sim 1.4 \times 10^{19}$ molecule m^{-3}, and the corresponding partial pressure (P) of reaction gas was 30–57 mPa for the different valve-opening times.

Theoretical methods. Theoretical calculations were conducted using the generalized gradient approximation (GGA) BP86 functional[58,59] with the DFT-D3 dispersion correction[60] included. All the structure optimization and reaction coordination research were performed using the def2-TZVP basis sets[61,62] implemented in the Gaussian 09 programme[63]. The BP86 functional has been proved to provide accurate geometries and spin states for transition metals including vanadium[44,64,65]. We investigated a large number of possible structures, including the structures previously found for vanadium clusters[66–68], vanadium hydrates[40,46,69], and vanadium oxides[70,71]. Multiple spin configurations and vibrational frequency calculations were examined to ensure that the lowest energy structures and multiplicity were correctly identified. The convergence threshold for the RMS forces in the optimization was set to be 10^{-4} a.u., and all the procedures meet this criterion. All energies in this work were corrected for the vibrational zero-point energies. For the determination of transition structures (TSs), we applied both the Berny algorithm and synchronous transit guided quasi-Newton (STQN) methods. The initial approximate transition structures were obtained by relaxed PES scans using an appropriate internal coordinate. For the candidate TSs, intrinsic reaction-coordinate (IRC) calculations were conducted to check the connection of a TS with both-side local minima; also, the number of vibrational imaginary frequencies was examined and the ascertained TSs had only one imaginary frequency. The orbital patterns are plotted via the software package of visual molecular dynamics (VMD)[72].

Data availability

All data supporting the findings of this study are available within the paper and its supplementary information.

Received: 19 May 2020; Accepted: 6 October 2020;
Published online: 30 October 2020

References

1. Lasia, A. *Hydrogen Evolution Reaction* (John Wiley & Sons, Ltd, 2010).
2. Zhu, Y. et al. Unusual synergistic effect in layered Ruddlesden–Popper oxide enables ultrafast hydrogen evolution. *Nat. commun.* **10**, 149 (2019).
3. de Levie, R. The electrolysis of water. *J. Electroanal. Chem.* **476**, 92–93 (1999).
4. Buttler, A. & Spliethoff, H. Current status of water electrolysis for energy storage, grid balancing and sector coupling via power-to-gas and power-to-liquids: a review. *Renew. Sustain. Energ. Rev.* **82**, 2440–2454 (2018).
5. Tong, W. et al. Electrolysis of low-grade and saline surface water. *Nat. Energy* **5**, 367–377 (2020).
6. del Valle, F. et al. Influence of Zn concentration in the activity of $Cd_{1-x}Zn_xS$ solid solutions for water splitting under visible light. *Catal. Today* **143**, 51–56 (2009).
7. Kiwi, J. & Gratzel, M. Protection, size factors, and reaction dynamics of colloidal redox catalysts mediating light-induced hydrogen evolution from water. *J. Am. Chem. Soc.* **101**, 7214–7217 (1979).
8. Navarro, R. M., del Valle, F., Villoria de la Mano, J. A., Álvarez-Galván, M. C. & Fierro, J. L. G. in *Advances in Chemical Engineering* Vol. 36 (eds de Lasa, H. I. & Rosales, B. S.) 111–143 (Academic Press, 2009).
9. Funk, J. E. Thermochemical hydrogen production: past and present. *Int. J. Hydrog. Energy* **26**, 185–190 (2001).
10. McClean, R. E., Nelson, H. H. & Campbell, M. L. Kinetics of the reaction Al ($^2P^0$) + H_2O over an extended temperature range. *J. Phys. Chem.* **97**, 9673–9676 (1993).
11. Alvarez-Barcia, S. & Flores, J. R. The interaction of Al atoms with water molecules: a theoretical study. *J. Chem. Phys.* **131**, 174307 (2009).
12. Álvarez-Barcia, S. & Flores, J. R. A theoretical study of the dynamics of the Al + H_2O reaction in the gas-phase. *Chem. Phys.* **382**, 92–97 (2011).
13. Zhang, C. X. et al. A synthetic Mn_4Ca-cluster mimicking the oxygen-evolving center of photosynthesis. *Science* **348**, 690–693 (2015).
14. Giri, A. K., Roberts, A. J., Hornbuckle, B. C., Grendahl, S. M. & Darling, K. A. Aluminum based nanogalvanic compositions useful for generating hydrogen gas and low temperature processing thereof. US patent US20190024216A1 (2019).
15. Beyer, M. et al. Fragmentation and intracluster reactions of hydrated aluminum cations Al + $(H_2O)_n$, $n = 3$–50. *J. Am. Chem. Soc.* **118**, 7386–7389 (1996).
16. Reinhard, B. M. & Niedner-Schatteburg, G. H_2 Elimination from hydrated aluminum clusters: acid–base reaction mediated by intracluster proton transfer. *J. Phys. Chem. A* **106**, 7988–7992 (2002).
17. Siu, C.-K., Liu, Z.-F. & Tse, J. S. Ab initio studies on $Al^+(H_2O)_n$, $HAlOH^+(H_2O)_{n-1}$, and the size-dependent H2 elimination reaction. *J. Am. Chem. Soc.* **124**, 10846–10860 (2002).
18. Roach, P. J., Woodward, W. H., Castleman, A. W. Jr., Reber, A. C. & Khanna, S. N. Complementary active sites cause size-selective reactivity of aluminum cluster anions with water. *Science* **323**, 492–495 (2009).
19. Breiter, M. W. Voltammetric study of the volmer reaction on platinum in sulfuric acid solution. I. Dependence of the exchange current density upon the hydrogen coverage at 30 °C. *J. Phys. Chem.* **68**, 2249–2253 (1964).
20. Zhang, T. & Anderson, A. B. Hydrogen oxidation and evolution on platinum electrodes in base: theoretical study. *J. Phys. Chem. C* **111**, 8644–8648 (2007).
21. Reber, A. C., Khanna, S. N., Roach, P. J., Woodward, W. H. & Castleman, A. W. Jr. Reactivity of aluminum cluster anions with water: origins of reactivity and mechanisms for H_2 release. *J. Phys. Chem. A* **114**, 6071–6081 (2010).
22. Ohmura, S. et al. Reaction of aluminum clusters with water. *J. Chem. Phys.* **134**, 244702 (2011).

23. Álvarez-Barcia, S. & Flores, J. R. How fast do microhydrated al clusters react: a theoretical study. *J. Phys. Chem. C* **115**, 24849–24857 (2011).
24. Álvarez-Barcia, S. & Flores, J. R. Size, adsorption site, and spin effects in the reaction of Al clusters with water molecules: Al_{17} and Al_{28} as examples. *J. Phys. Chem. A* **116**, 8040–8050 (2012).
25. Alvarez-Barcia, S. & Flores, J. R. Hydrogen migration dynamics in hydrated Al clusters: the Al_{17}–H_2O system As an example. *J. Chem. Phys.* **140**, 084313 (2014).
26. Luo, Z., Castleman, A. W. Jr. & Khanna, S. N. Reactivity of metal clusters. *Chem. Rev.* **116**, 14456–14492 (2016).
27. Luo, Z., Smith, J. C., Woodward, W. H. & Castleman, A. W. Jr. Reactivity of aluminum clusters with water and alcohols: competition and catalysis? *J. Phys. Chem. Lett.* **3**, 3818–3821 (2012).
28. Pembere, A. M. S., Liu, X., Ding, W. & Luo, Z. How partial atomic charges and bonding orbitals affect the reactivity of aluminum clusters with water? *J. Phys. Chem. A* **122**, 3107–3114 (2018).
29. Wang, H. Z., Leung, D. Y. C., Leung, M. K. H. & Ni, M. A review on hydrogen production using aluminum and aluminum alloys. *Renew. Sust. Energ. Rev.* **13**, 845–853 (2009).
30. Woodall, J. M. et al. In *Materials Innovations in an Emerging Hydrogen Economy*, Vol. 202 *Ceramic Transactions* (eds Wicks, G. G. & Simon, J.) 121–127 (John Wiley and Sons, 2009).
31. Li, F. et al. Mechanisms of H_2 generation for metal doped $Al_{16}M$ (M = Mg and Bi) clusters in water. *Int. J. Hydrog. Energy* **38**, 6930–6937 (2013).
32. Li, K. N., Yang, C. L., Wang, M. S., Ma, X. G. & Wang, L. Z. Extraction of H_2 from H_2O molecule using a small Al_6Si cluster. *Int. J. Hydrog. Energy* **41**, 17858–17863 (2016).
33. Zhang, H., Cui, C. & Luo, Z. The doping effect of 13-atom iron clusters on water adsorption and O–H bond dissociation. *J. Phys. Chem. A* **123**, 4891–4899 (2019).
34. Chen, J. & Luo, Z. Single-point attack of two H_2O molecules towards a Lewis acid site on the $GaAl_{12}$ clusters for hydrogen evolution. *ChemPhysChem* **20**, 499–505 (2019).
35. Clemmer, D. E., Sunderlin, L. S. & Armentrout, P. B. Ammonia activation by Sc^+ and Ti^+—electronic and translational energy-dependence. *J. Phys. Chem.* **94**, 3008–3015 (1990).
36. Chen, Y. M., Clemmer, D. E. & Armentrout, P. B. Kinetic and electronic-energy dependence of the reactions of Sc^+ and Ti^+ with D_2O. *J. Phys. Chem.* **98**, 11490–11498 (1994).
37. Chiodo, S. et al. Theoretical study of two-state reactivity of transition metal cations: the "difficult" case of iron ion interacting with water, ammonia, and methane. *J. Phys. Chem. A* **108**, 1069–1081 (2004).
38. Beyer, M. K. Hydrated metal ions in the gas phase. *Mass Spectrom. Rev.* **26**, 517–541 (2007).
39. Cheng, P., Koyanagi, G. K. & Bohme, D. K. Heavy water reactions with atomic transition-metal and main-group cations: gas phase room-temperature kinetics and periodicities in reactivity. *J. Phys. Chem. A* **111**, 8561–8573 (2007).
40. Irigoras, A., Fowler, J. E. & Ugalde, J. M. Reactivity of $Sc^+(^3D,^1D)$ and $V^+(^5D,^3F)$: reaction of Sc^+ and V^+ with Water. *J. Am. Chem. Soc.* **121**, 574–580 (1999).
41. Fox, B. S. et al. Black body radiation induced hydrogen formation in hydrated vanadium cations $V^+(H_2O)$n. *Phys. Chem. Chem. Phys.* **4**, 2224–2228 (2002).
42. van der Linde, C. & Beyer, M. K. Reactions of $M^+(H_2O)_n$, $n < 40$, M = V, Cr, Mn, Fe, Co, Ni, Cu, and Zn, with D_2O reveal water activation in Mn+(H2O)n. *J. Phys. Chem. A* **116**, 10676–10682 (2012).
43. Clemmer, D. E., Chen, Y. M., Aristov, N. & Armentrout, P. B. Kinetic and electronic-energy dependence of the reaction of V^+ with D_2O. *J. Phys. Chem.* **98**, 7538–7544 (1994).
44. Zhang, H. et al. Furthering the reaction mechanism of cationic vanadium clusters towards oxygen. *Phys. Chem. Chem. Phys.* **21**, 11234–11241 (2019).
45. Kramida, A., Ralchenko, Y., Reader, J. & Team, N. A. *NIST Atomic Spectra Database* (*Version 5.6.1*) https://physics.nist.gov/asd (2018).
46. Meza, B., Miranda, P. & Castro, M. Structural and electronic properties of hydrated V_nH_2O and $V_n{}^+H_2O$, $n \leq 13$, systems. *J. Phys. Chem. C* **121**, 4635–4649 (2017).
47. Zhang, H. et al. An integrated instrument of DUV-IR photoionization mass spectrometry and spectroscopy for neutral clusters. *Rev. Sci. Instrum.* **90**, 073101 (2019).
48. Boodts, J. C. F. & Trasatti, S. Hydrogen evolution on iridium oxide cathodes. *J. Appl. Electrochem.* **19**, 255–262 (1989).
49. Cui, C., Luo, Z. & Yao, J. Enhanced catalysis of Pt3 clusters supported on graphene for N–H bond dissociation. *CCS Chem.* **1**, 215–225 (2019).
50. Knight, W. D. et al. Electronic shell structure and abundances of sodium clusters. *Phys. Rev. Lett.* **52**, 2141–2143 (1984).
51. Katakuse, I. et al. Mass distributions of copper, silver and gold clusters and electronic shell structure. *Int. J. Mass Spectrom. Ion-. Process.* **67**, 229–236 (1985).
52. Luo, Z. et al. Spin accommodation and reactivity of silver clusters with oxygen: the enhanced stability of $Ag_{13}{}^-$. *J. Am. Chem. Soc.* **134**, 18973–18978 (2012).
53. Balducci, G., Gigli, G. & Guido, M. Thermochemical properties of the gaseous molecules VO, VO_2, and V_2O_4. *J. Chem. Phys.* **79**, 5616–5622 (1983).
54. Xu, J., Rodgers, M. T., Griffin, J. B. & Armentrout, P. B. Guided ion beam studies of the reactions of $V_n{}^+$ ($n = 2$–17) with O_2: bond energies and dissociation pathways. *J. Chem. Phys.* **108**, 9339–9350 (1998).
55. Armentrout, P. B. Guided ion beam studies of transition metal–ligand thermochemistry. *Int. J. Mass Spectrom.* **227**, 289–302 (2003).
56. Schröder, D., Shaik, S. & Schwarz, H. Two-state reactivity as a new concept in organometallic chemistry. *Acc. Chem. Res.* **33**, 139–145 (2000).
57. Zhang, H. et al. Formation of $Al^+(C_6H_6)_{13}$: the origin of magic number in metal–benzene clusters determined by the nature of the core. *CCS Chem.* **1**, 571–581 (2019).
58. Perdew, J. P. Density-functional approximation for the correlation energy of the inhomogeneous electron gas. *Phys. Rev. B* **33**, 8822–8824 (1986).
59. Becke, A. D. Density-functional exchange-energy approximation with correct asymptotic behavior. *Phys. Rev. A* **38**, 3098–3100 (1988).
60. Grimme, S., Antony, J., Ehrlich, S. & Krieg, H. A consistent and accurate ab initio parametrization of density functional dispersion correction (DFT-D) for the 94 elements H-Pu. *J. Chem. Phys.* **132**, 154104–154122 (2010).
61. Schäfer, A., Huber, C. & Ahlrichs, R. Fully optimized contracted gaussian basis sets of triple zeta valence quality for atoms Li to Kr. *J. Chem. Phys.* **100**, 5829–5835 (1994).
62. Weigend, F. & Ahlrichs, R. Balanced basis sets of split valence, triple zeta valence and quadruple zeta valence quality for h to rn: design and assessment of accuracy. *Phys. Chem. Chem. Phys.* **7**, 3297–3305 (2005).
63. Frisch, M. J. et al. Gaussian 09 Rev. E.01 (Wallingford, CT, 2009).
64. Gorelsky, S. I. Complexes with a single metal–metal bond as a sensitive probe of quality of exchange-correlation functionals. *J. Chem. Theory Comput.* **8**, 908–914 (2012).
65. Jensen, K. P., Roos, B. O. & Ryde, U. Performance of density functionals for first row transition metal systems. *J. Chem. Phys.* **126**, 014103 (2007).
66. Wu, X. & Ray, A. K. A density functional study of small neutral and cationic vanadium clusters V_n and $V_n{}^+$ ($N = 2$–9). *J. Chem. Phys.* **110**, 2437–2445 (1999).
67. Fielicke, A. et al. Structure determination of isolated metal clusters via far-infrared spectroscopy. *Phys. Rev. Lett.* **93**, 023401 (2004).
68. Ratsch, C. et al. Structure determination of small vanadium clusters by density-functional theory in comparison with experimental far-infrared spectra. *J. Chem. Phys.* **122**, 124302 (2005).
69. Kasalová, V., Allen, W. D., Schaefer, H. F., Pillai, E. D. & Duncan, M. A. Model systems for probing metal cation hydration: the $V^+(H_2O)$ and $ArV^+(H_2O)$ complexes. *J. Phys. Chem. A* **111**, 7599–7610 (2007).
70. Engeser, M., Weiske, T., Schroder, D. & Schwarz, H. Oxidative degradation of small cationic vanadium clusters by molecular oxygen: on the way from $V_n{}^+$ ($n = 2$–5) to $VO_m{}^+$ ($m = 1$, 2). *J. Phys. Chem. A* **107**, 2855–2859 (2003).
71. Wang, H. Q., Li, H. F. & Kuang, X. Y. Probing the structural and electronic properties of small vanadium monoxide clusters. *Phys. Chem. Chem. Phys.* **14**, 5272–5283 (2012).
72. Humphrey, W., Dalke, A. & Schulten, K. VMD: visual molecular dynamics. *J. Mol. Graph.* **14**, 33–38 (1996).
73. Glendening, E. D. et al. *NBO 6.0*: Natural bond orbital analysis program. *Journal of Computational Chemistry* **34**, 1429–1437 (2013).

Acknowledgements

Financial support for this work was provided by the National Natural Science Foundation of China (21722308), the National Project Development of Advanced Scientific Instruments Based on Deep Ultraviolet Laser Source (Y31M0112C1), and the Key Research Programme of Frontier Sciences (QYZDBSSW-SLH024).

Author contributions

H.Z., Y.J. and L.G. conducted the experiments; H.W., H.Z. and B.Y. conducted the calculations; Z.L. and K.H. contributed to the design of this project. All authors contributed to data analysis and writing the manuscript.

Competing interests

The authors declare no competing interests.

Additional information

Supplementary information is available for this paper at https://doi.org/10.1038/s42004-020-00396-9.

Correspondence and requests for materials should be addressed to Z.L.

Reprints and permission information is available at http://www.nature.com/reprints

Publisher's note Springer Nature remains neutral with regard to jurisdictional claims in published maps and institutional affiliations.